PROCEEDINGS OF SCIENCE

Precision QCD calculations for vector boson observables

Thomas Gehrmann[a,*]

[a] *Universität Zürich, Physik-Institut, Winterthurerstrasse 190, CH-8057 Zürich, Switzerland*

E-mail: thomas.gehrmann@uzh.ch

Vector boson production is a classical benchmark process at hadron colliders, where it has been measured to high accuracy. We discuss recent progress on precision calculations for vector boson production at NNLO and N3LO in QCD and highlight the phenomenological impact of the newly derived corrections.

16th International Symposium on Radiative Corrections: Applications of Quantum Field Theory to Phenomenology (RADCOR2023)
28th May - 2nd June, 2023
Crieff, Scotland, UK

*Speaker

PoS(RADCOR2023)060

1. Introduction

The production of lepton-antilepton pairs in hadron-hadron scattering mediated by a virtual photon or a weak gauge boson (Drell-Yan process [1], DY) can be measured experimentally to extremely high precision. Extensive efforts have been made to produce theoretical predictions of similar accuracy. It plays a crucial role in determinations of parton distribution functions (PDFs) and Standard-Model (SM) electroweak (EW) parameters.

The theoretical description of Drell-Yan differential distributions relies on perturbation theory in the Standard Model couplings, which is available to next-to-leading order (NLO) in the EW theory, next-to-next-to-leading order (NNLO) in QCD [2, 3], and with mixed QCD+EW corrections [4–9]. Recently, third-order (N3LO) QCD corrections were derived for the fully inclusive Drell-Yan coefficient functions [10–12], for single-differential distributions [13] and for fiducial cross sections [14–16], thus opening up the path towards fully differential predictions at this order.

In this talk, we will review recent developments towards high-precision predictions for DY observables at the LHC, including precision phenomenology with triple-differential Drell-Yan measurements [17], first steps towards fully differential predictions at N3LO QCD [13–15] and the inclusion of quark-singlet axial-vector contributions [18, 19] at two and three loops.

2. Triple-differential Drell-Yan cross section

At Born level, the di-lepton pair is produced at vanishing transverse momentum, and its kinematics can be described by three variables: the di-lepton invariant mass m_{ll}, di-lepton rapidity $y_{ll}$and the scattering angle $\cos\theta^*$, which is defined in the Collins-Soper (CS) frame [20]:

$$\frac{\mathrm{d}^3\sigma}{\mathrm{d}m_{ll}\mathrm{d}y_{ll}\mathrm{d}\cos\theta^*} \tag{1}$$

The ATLAS collaboration performed a measurement [21] of the triply-differential Drell-Yan cross section (1) at $\sqrt{s} = 8$ TeV, based on 20.2 fb^{-1} of data taken in 2012 using combined electron and muon decay channels. Depending on the rapidities of the individual leptons, the measurement is divided into two regions, defined by different selection criteria; a central-central (CC) region where both leptons are observed in the central rapidity region of the ATLAS detector, and a central-forward (CF) region where one lepton is found in the central region whilst the other is measured in the forward-detector region. The full fiducial cuts and binnings are summarised in Tables 1 and 2.

The definition of the fiducial cuts on individual lepton momenta contrasts with the use of di-lepton variables in the definition of the triple-differential cross section. This interplay of kinematical variables leads to an intricate structure of the measurement regions, potentially implying non-trivial acceptance effects and an enhanced sensitivity to extra radiation from higher-order corrections.

At Born level, the kinematics are particularly simple, and serve as a good illustration of how phase-space constraints can be induced by fiducial cuts. One can then use this to classify the measurement bins in $(|y_{ll}|, \cos\theta^*)$-space into three categories, depending on whether the associated fiducial regions can be fully accessed, partially accessed, or are completely forbidden at LO. The bin classifications for the central-central region are shown on the left of Figure 1 where, as one would expect, the majority of bins in the central region ($y_{ll} \sim 0$) are fully allowed, while beyond

Central-Central	Central-Forward
$p_{\mathrm{T}}^{l} > 20$ GeV	$p_{\mathrm{T,F}}^{l} > 20$ GeV $\quad p_{\mathrm{T,C}}^{l} > 25$ GeV
$\lvert y^{l}\rvert < 2.4$	$2.5 < \lvert y_{\mathrm{F}}^{l}\rvert < 4.9 \quad \lvert y_{\mathrm{C}}^{l}\rvert < 2.4$
$46\ \mathrm{GeV} < \mathrm{m_{ll}} < 200\ \mathrm{GeV}$	$66\ \mathrm{GeV} < \mathrm{m_{ll}} < 150\ \mathrm{GeV}$

Table 1: Selection criteria for the central-central and central-forward fiducial regions in the ATLAS measurement of [21].

Observable	Central-Central	Central-Forward
m_{ll} [GeV]	[46, 66, 80, 91, 102, 116, 150, 200]	[66, 80, 91, 102, 116, 150]
$\lvert y_{ll}\rvert$	[0, 0.2, 0.4, 0.6, 0.8, 1, 1.2, 1.4, 1.6, 1.8, 2, 2.2, 2.4]	[1.2, 1.6, 2, 2.4, 2.8, 3.6]
$\cos\theta^*$	$[-1, -0.7, -0.4, 0, 0.4, 0.7, 1]$	$[-1, -0.7, -0.4, 0, 0.4, 0.7, 1]$
Total Bin Count	504	150

Table 2: Binnings for the central-central and central-forward fiducial regions in the ATLAS measurement of [21].

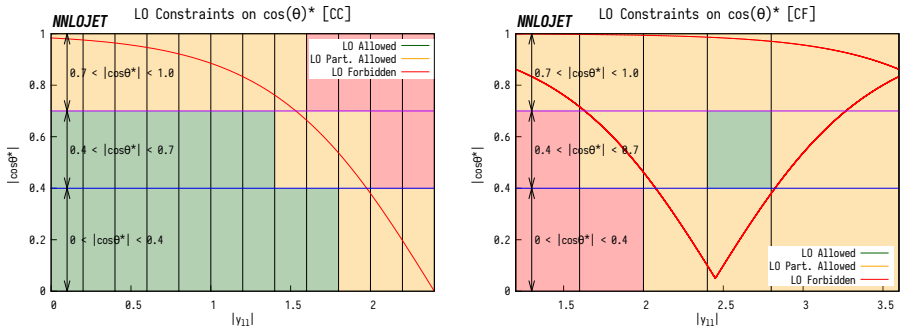

Figure 1: Bin classifications at LO for the central-central (left) and central-forward (right) triple-differential Drell-Yan fiducial region in the ($|y_{ll}|$, $\cos\theta^*$) plane. Overlaid are the measurement bins, integrated over m_{ll}.

$|y_{ll}| = 1.4$ the restrictions take effect. For the central-forward region, Figure 1 (right), one can see that a more dramatic effect of the fiducial cuts, which restrict the fully allowed phase space to non-central values of $|\cos\theta^*|$.

The kinematical regions that are forbidden at Born level can be accessed if the lepton pair acquires some non-vanishing transverse momentum Q_{T} from initial state radiation. Consequently, the theory predictions for these forbidden bins start only at NLO in QCD, and they are associated with large theory uncertainties even at NNLO. This effective Q_{T}-cut can however be employed to extend the accuracy of the fixed-order theoretical predictions for the Born-forbidden bins by using calculations of vector-boson-plus-jet in a similar manner as for the p_{T}^{V} spectrum, since the requirement for a non-zero Q_{T} implicitly enforces partonic radiation. Fully differential results for the vector-boson-plus-jet process are known to α_s^3, corresponding to the NNLO QCD corrections [16, 22, 23]. Most recently, the α_s^3 corrections were also computed to differential DY production [13–16], where they correspond to N3LO QCD. However, these N3LO calculations are not yet sufficiently

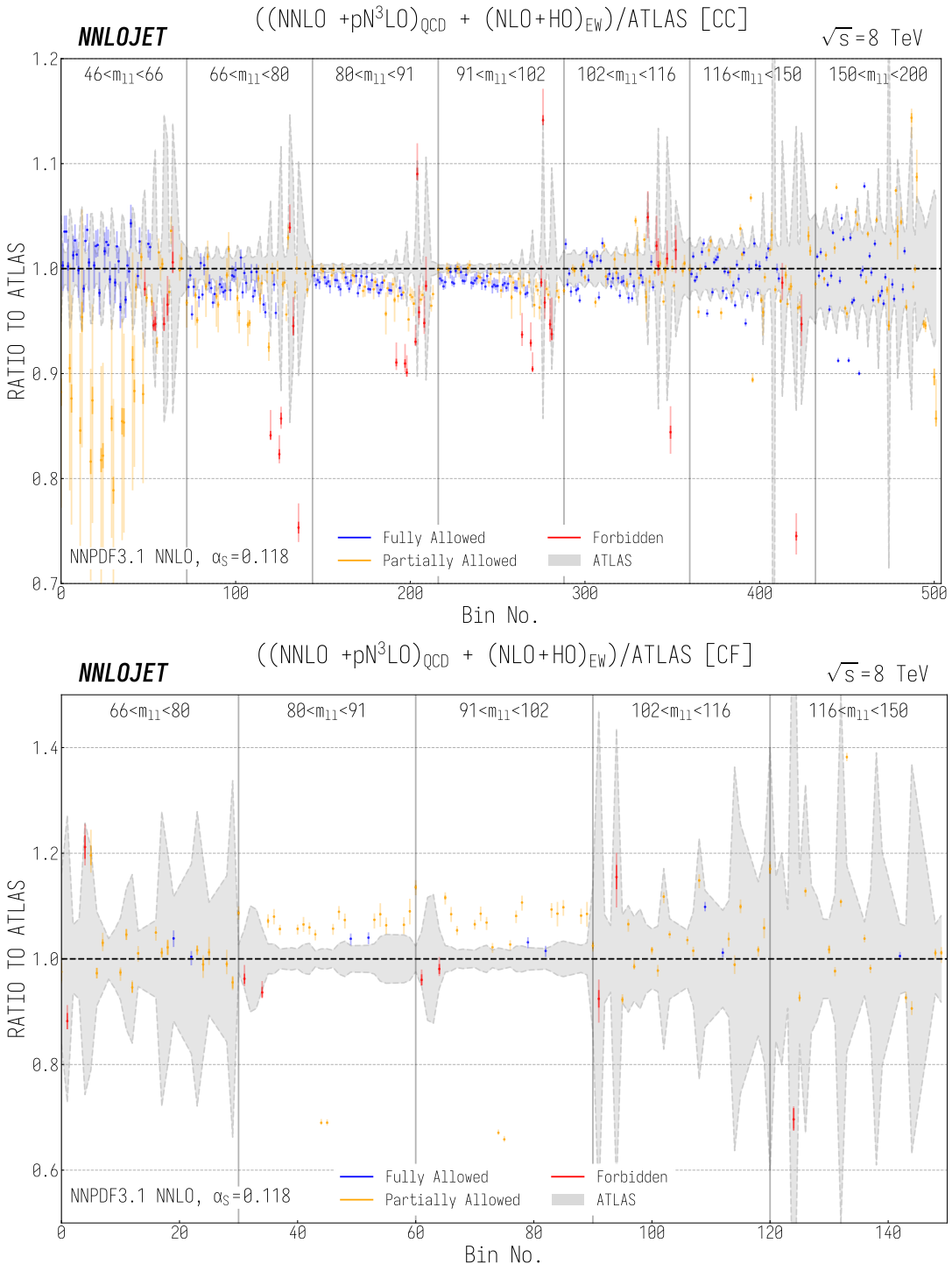

Figure 2: Ratio of (NNLO+pN3LO)$_{\rm QCD}$ + (NLO+HO)$_{\rm EW}$ predictions to ATLAS data in the central-central (top panel) and central-forward (bottom panel) region of the triple differential DY cross section. Light error bars correspond to scale-variation uncertainties and dark error bars correspond to statistical uncertainties. The grey shaded region shows the experimental uncertainty of the ATLAS measurement. The bin number is as defined by increments in $|\cos\theta^*|$, followed by $|y_{ll}|$, followed by m_{ll}, as described in [17].

efficient to yield the multi-differential distributions as considered here. By restricting the α_s^3 contributions to the forbidden bins, where the triple virtual contribution which lies in the Born phase space does not contribute, this represents an improvement equivalent to extending the predictions to N3LO accuracy in these bins.

NNLO and partial N3LO QCD predictions are calculated using existing implementations of the vector-boson and vector-boson-plus-jet processes in NNLOJET [22]. Fixed-order electroweak corrections are computed using a modified version of the `Z_ew-BMNNPV` code [24] in POWHEG-BOX [25]. The computation is performed at NLO EW, including the leading higher-order (HO) corrections to $\Delta\rho$ and $\Delta\alpha$ described in [26].

The ratio to data for both the CC and CF regions is shown in Figure 2. In the CC region, we observe that the data are well-described by the theory predictions. In comparison to the NNLO QCD predictions [17], the Born-forbidden bins are described considerably better, and with substantially lower theory uncertainty. The EW corrections are quite uniform in $y_{ll}$and $\cos\theta^*$, but display a strong dependence on m_{ll}. They lead to an improved description of the normalization of the data. The same is not true for the CF region, where we see a consistent over-shooting of the data with respect to the theory prediction. Here the predictions become very sensitive to the high-x valence quark distribution, and these data can potentially serve in improved PDF determinations in the future.

3. Towards N3LO in Drell-Yan observables

Most recently, important steps were taken in the computation of differential N3LO QCD corrections to DY observables. These calculations [13–16] are all based on the Q_T-subtraction formalism [27]:

$$\mathrm{d}\sigma_{\mathrm{DY}}^{\mathrm{N3LO}} = \mathcal{F}_{\mathrm{DY}}^{\mathrm{N3LO}} \otimes \mathrm{d}\sigma_{\mathrm{DY}}^{\mathrm{LO}}|_{Q_T<Q_T^{\mathrm{cut}}} + \mathrm{d}\sigma_{\mathrm{DY+jet}}^{\mathrm{NNLO}}|_{Q_T>Q_T^{\mathrm{cut}}}, \tag{2}$$

where a slicing parameter Q_T^{cut} is introduced to separate unresolved and resolved contributions. The independence of the results on the unphysical slicing parameter Q_T^{cut} serves as a strong check.

The unresolved contribution $\mathcal{F}_{\mathrm{DY}}^{\mathrm{N3LO}} \otimes \mathrm{d}\sigma_{\mathrm{DY}}^{\mathrm{LO}}|_{Q_T<Q_T^{\mathrm{cut}}}$ denotes the fixed-order prediction for producing a DY pair with transverse momentum Q_T less than Q_T^{cut}. It can be expanded into logarithmic terms $\alpha_s^m \ln^n(Q_T^{\mathrm{cut}}/m_{ll})$ and constant terms. All logarithmic terms can be predicted through to N3LO [28, 29] using the rapidity renormalization group formalism [30]. The key ingredients to achieve N3LO accuracy for color-singlet production are the constant terms. They arise from the boundary conditions for the renormalization group equation, namely the rapidity-divergent transverse-momentum-dependent soft function [31] and beam functions [32–34] at three loops.

Applying the Q_T-subtraction method described above, we computed the N3LO corrections to the rapidity distribution in neutral-current DY production [13] and independently rederived the inclusive coefficient function [10] at this order. Subsequently, we used this approach to compute fiducial cross sections in neutral-current [14] and charged-current [15] Drell-Yan production. The latter process corresponds to W-boson production, and the differential distributions derived from it enable precision measurements of the W-boson mass.

As an example, Fig. 3 presents the normalized $\mathrm{W}^{\pm}$ boson transverse mass distribution at the Tevatron. With the newly computed N3LO corrections, it establishes a new state-of-the-art in the

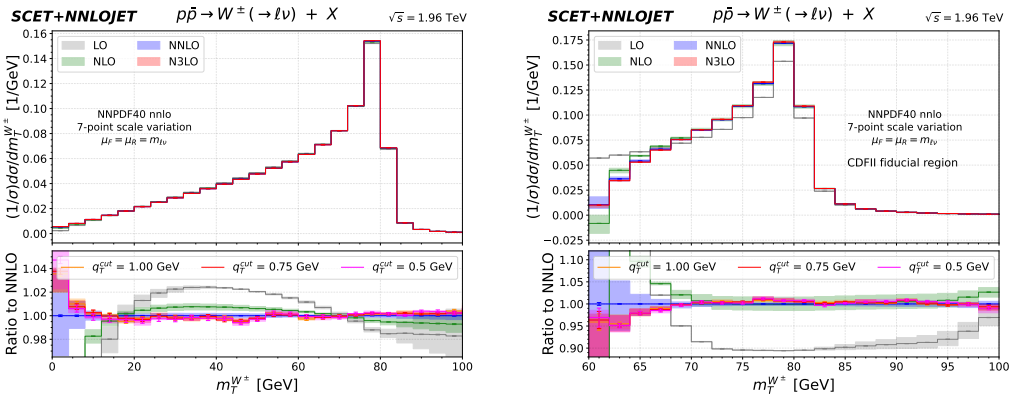

Figure 3: Normalised $W^{\pm}$ transverse mass distribution from LO to N3LO accuracy at the Tevatron without (left) and with (right) CDFII fiducial cuts. The colored bands represent theory uncertainties from 7-point scale variation. The bottom panel is the ratio with respect to NNLO, with different technical parameters Q_T^{cut}.

precise description of this observable. The inclusive distribution without fiducial cuts is displayed in the left frame, while the fiducial cuts on charged lepton and neutrino of the CDFII analysis [35] are applied in the right frame: $p_{T,l}, E_{T,\nu} \in [30, 55]$ GeV, $|\eta_l| < 1$ and $p_{T,W^{\pm}} < 15$ GeV. At N3LO, corrections are very uniform in the peak region for both inclusive and fiducial distribution, while displaying some kinematical dependence at low $m_T^{W^{\pm}}$ below 12 GeV in the inclusive distribution and below 68 GeV in the fiducial distribution. Starting from NNLO, we observe scale uncertainties at the level of below $\pm 1\%$, thus thoroughly establishing the perturbative stability of this observable.

4. Axial-vector contributions

Up to now, all NNLO QCD calculations of Z+jet production at the LHC [16, 22, 23] discarded the axial-vector pure-singlet contributions, due to the lack of the corresponding two-loop axial-vector amplitudes for crossings of $Z \to q\bar{q}g$. The very same axial-vector pure-singlet amplitudes also contribute to the third-order (N3LO) corrections to Z boson production at hadron colliders, together with the corresponding three-loop quark singlet axial-vector form factor [18, 36]. Their contribution to the inclusive Z boson coefficient functions at N3LO has been computed most recently [11] by combining loop and phase space integrations, but not allowing direct access to the underlying two-loop amplitudes. The main obstacle to their calculation was the tensor decomposition of the helicity amplitudes, which was up to now limited to vector-couplings only.

It was shown in [37, 38], by working in the 't Hooft-Veltman dimensional regularisation scheme, that a tensor decomposition can be performed by assuming that all external states are in exactly $d = 4$ space-time dimensions, since all remaining evanescent tensor structures turn out not to contribute to the helicity amplitudes, even in $d = 4 - 2\epsilon$.

For the Z+jet amplitudes, three basis vectors can be chosen to be the three independent momenta p_1^{μ}, p_2^{μ}, p_3^{μ}, such that the natural fourth independent vector is the orthogonal, axial-vector

$$\epsilon^{\nu\rho\sigma\mu} p_{1\nu} p_{2\rho} p_{3\sigma} = \epsilon^{p_1 p_2 p_3 \mu} = v_A^{\mu}, \tag{3}$$

where $\epsilon^{\mu\nu\rho\sigma}$ is the Levi-Civita symbol. We note that $p_i \cdot v_A = 0$.

Discarding trivial normalization factors, the $Z(p_4,\mu)q(p_1)\bar{q}(p_2)g(p_3,\nu)$ amplitudes can be decomposed as

$$\begin{aligned}A^{\mu\nu} = {} & \bar{u}(p_2)\not{p}_3 u(p_1)\Big[F_1 p_1^\mu p_1^\nu + F_2 p_2^\mu p_1^\nu + F_3 g^{\mu\nu} + G_1 p_1^\mu v_A^\nu + G_2 p_2^\mu v_A^\nu + G_3 v_A^\mu p_1^\nu\Big] \\ & + \bar{u}(p_2)\gamma^\nu u(p_1)\Big[F_4 p_1^\mu + F_5 p_2^\mu\Big] + \bar{u}(p_2)\gamma^\mu u(p_1) F_6 p_1^\nu \\ & + \bar{u}(p_2)\not{\gamma}_A u(p_1)\Big[G_4 p_1^\mu p_1^\nu + G_5 p_2^\mu p_1^\nu\Big] + G_6\Big[\bar{u}(p_2)\gamma^\mu u(p_1) v_A^\nu + \bar{u}(p_2)\gamma^\nu u(p_1) v_A^\mu\Big], \end{aligned} \tag{4}$$

in terms of vector and axial-vector form factors F_i and G_j. This basis allows for a consistent application of the Larin scheme [39] for axial couplings in dimensional regularization in the computation of the associated form factors. In this new basis, we rederived [19] the non-singlet helicity amplitudes at two loops, confirming the earlier results [40, 41] and explicitly demonstrating the equivalence of vector and axial-vector amplitudes in the non-singlet case, after renormalization and IR factorization.

In the pure-singlet axial-vector amplitudes, the vector boson couples to an internal quark loop. These amplitudes are affected by the axial anomaly, which cancels in the electroweak Standard Model upon summation over weak isospin doublets. We computed the two-loop pure-singlet axial-vector form factors [19], separately for massless internal quarks and in a large-mass expansion for massive internal quarks, and recovering in both cases the correct universal divergent behaviour of the axial anomaly. Subleading terms in the large-mass expansion were also computed to demonstrate the internal consistency of the approach. The combination of massless and massive internal quarks describes the pure-singlet axial-vector contribution from top-bottom mass splitting.

5. Summary

In this talk, we discussed recent progress on precision calculations for vector boson observables. We highlighted the impact of fiducial event selection cuts on multi-differential Drell-Yan distributions, which lead to a complicated interplay between single-lepton and lepton-pair variables, thereby excluding a substantial fraction of the phase space at Born level. The theoretical description of the resulting fiducial distributions requires higher-order QCD corrections at NNLO and beyond, accounting for extra partonic radiation that is required to fully cover the phase space of the measurement. Single-differential Drell-Yan distributions can now be computed to N3LO, thereby establishing theory predictions at sub-per-cent level accuracy. With this increase in accuracy, numerically subleading contributions start to become relevant, including singlet axial-vector corrections to the scattering amplitudes, relating to the top-bottom quark mass splitting. Owing to recent progress on the tensor decomposition of axial-vector amplitudes, the full set of scattering amplitudes relevant to DY production at N3LO is now available and ready to to be applied to precision phenomenology in lepton pair production at the LHC.

Acknowledgments

I would like to thank Xuan Chen, Aude Gehrmann-De Ridder, Nigel Glover, Alexander Huss, Pier Monni, Tiziano Peraro Christian Preuss, Emanuele Re, Luca Rottoli, Lorenzo Tancredi, Paolo

Torrielli, Duncan Walker, Tong-Zhi Yang and HuaXing Zhu for very pleasant collaborations on the different works presented in this talk. This work was supported in part by the Swiss National Science Foundation (SNF) under contract 200020-204200,and by the European Research Council (ERC) under the European Union's research and innovation programme grant agreement 101019620 (ERC Advanced Grant TOPUP).

References

[1] S. D. Drell and T.-M. Yan, *Phys. Rev. Lett.* **25** (1970) 316–320.

[2] K. Melnikov and F. Petriello, *Phys. Rev.* **D74** (2006) 114017, [hep-ph/0609070].

[3] S. Catani, L. Cieri, G. Ferrera, D. de Florian, and M. Grazzini, *Phys. Rev. Lett.* **103** (2009) 082001, [0903.2120].

[4] S. Dittmaier, A. Huss, and C. Schwinn, *Nucl. Phys.* **B904** (2016) 216–252, [1511.08016].

[5] R. Bonciani, F. Buccioni, N. Rana, I. Triscari, and A. Vicini, *Phys. Rev. D* **101** (2020) 031301, [1911.06200].

[6] S. Dittmaier, T. Schmidt, and J. Schwarz, *JHEP* **12** (2020) 201, [2009.02229].

[7] R. Bonciani, L. Buonocore, M. Grazzini, S. Kallweit, N. Rana, F. Tramontano, and A. Vicini, *Phys. Rev. Lett.* **128** (2022) 012002, [2106.11953].

[8] T. Armadillo, R. Bonciani, S. Devoto, N. Rana, and A. Vicini, *JHEP* **05** (2022) 072, [2201.01754].

[9] F. Buccioni, F. Caola, H. A. Chawdhry, F. Devoto, M. Heller, A. von Manteuffel, K. Melnikov, R. Röntsch, and C. Signorile-Signorile, *JHEP* **06** (2022) 022, [2203.11237].

[10] C. Duhr, F. Dulat, and B. Mistlberger, *Phys. Rev. Lett.* **125** (2020) 172001, [2001.07717].

[11] C. Duhr and B. Mistlberger, *JHEP* **03** (2022) 116, [2111.10379].

[12] J. Baglio, C. Duhr, B. Mistlberger, and R. Szafron, *JHEP* **12** (2022) 066, [2209.06138].

[13] X. Chen, T. Gehrmann, N. Glover, A. Huss, T.-Z. Yang, and H. X. Zhu, *Phys. Rev. Lett.* **128** (2022) 052001, [2107.09085].

[14] X. Chen, T. Gehrmann, E. W. N. Glover, A. Huss, P. F. Monni, E. Re, L. Rottoli, and P. Torrielli, *Phys. Rev. Lett.* **128** (2022) 252001, [2203.01565].

[15] X. Chen, T. Gehrmann, N. Glover, A. Huss, T.-Z. Yang, and H. X. Zhu, *Phys. Lett. B* **840** (2023) 137876, [2205.11426].

[16] T. Neumann and J. Campbell, *Phys. Rev. D* **107** (2023) L011506, [2207.07056].

[17] A. Gehrmann-De Ridder, T. Gehrmann, E. W. N. Glover, A. Huss, C. T. Preuss, and D. M. Walker, *JHEP* **05** (2023) 002, [2301.11827].

[18] T. Gehrmann and A. Primo, *Phys. Lett. B* **816** (2021) 136223, [2102.12880].

[19] T. Gehrmann, T. Peraro, and L. Tancredi, *JHEP* **02** (2023) 041, [2211.13596].

[20] J. C. Collins and D. E. Soper, *Phys. Rev.* **D16** (1977) 2219.

[21] **ATLAS** Collaboration, M. Aaboud et al. *JHEP* **12** (2017) 059, [1710.05167].

[22] A. Gehrmann-De Ridder, T. Gehrmann, E. W. N. Glover, A. Huss, and T. A. Morgan, *Phys. Rev. Lett.* **117** (2016) 022001, [1507.02850].

[23] R. Boughezal, J. M. Campbell, R. K. Ellis, C. Focke, W. T. Giele, X. Liu, and F. Petriello, *Phys. Rev. Lett.* **116** (2016) 152001, [1512.01291].

[24] L. Barze, G. Montagna, P. Nason, O. Nicrosini, F. Piccinini, and A. Vicini, *Eur. Phys. J.* **C73** (2013) 2474, [1302.4606].

[25] S. Alioli, P. Nason, C. Oleari, and E. Re, *JHEP* **06** (2010) 043, [1002.2581].

[26] S. Dittmaier and M. Huber, *JHEP* **01** (2010) 060, [0911.2329].

[27] S. Catani and M. Grazzini, *Phys. Rev. Lett.* **98** (2007) 222002, [hep-ph/0703012].

[28] X. Chen, T. Gehrmann, E. W. N. Glover, A. Huss, Y. Li, D. Neill, M. Schulze, I. W. Stewart, and H. X. Zhu, *Phys. Lett. B* **788** (2019) 425–430, [1805.00736].

[29] G. Billis, M. A. Ebert, J. K. L. Michel, and F. J. Tackmann, *Eur. Phys. J. Plus* **136** (2021) 214, [1909.00811].

[30] J.-Y. Chiu, A. Jain, D. Neill, and I. Z. Rothstein, *JHEP* **05** (2012) 084, [1202.0814].

[31] Y. Li and H. X. Zhu, *Phys. Rev. Lett.* **118** (2017) 022004, [1604.01404].

[32] M.-x. Luo, T.-Z. Yang, H. X. Zhu, and Y. J. Zhu, *Phys. Rev. Lett.* **124** (2020) 092001, [1912.05778].

[33] M. A. Ebert, B. Mistlberger, and G. Vita, *JHEP* **09** (2020) 146, [2006.05329].

[34] M.-x. Luo, T.-Z. Yang, H. X. Zhu, and Y. J. Zhu, *JHEP* **06** (2021) 115, [2012.03256].

[35] **CDF** Collaboration, T. Aaltonen et al. *Science* **376** (2022) 170–176.

[36] L. Chen, M. Czakon, and M. Niggetiedt, *JHEP* **12** (2021) 095, [2109.01917].

[37] T. Peraro and L. Tancredi, *JHEP* **07** (2019) 114, [1906.03298].

[38] T. Peraro and L. Tancredi, *Phys. Rev. D* **103** (2021) 054042, [2012.00820].

[39] S. A. Larin *Phys. Lett. B* **303** (1993) 113–118, [hep-ph/9302240].

[40] L. W. Garland, T. Gehrmann, E. W. N. Glover, A. Koukoutsakis, and E. Remiddi, *Nucl. Phys. B* **627** (2002) 107–188, [hep-ph/0112081].

[41] L. W. Garland, T. Gehrmann, E. W. N. Glover, A. Koukoutsakis, and E. Remiddi, *Nucl. Phys. B* **642** (2002) 227–262, [hep-ph/0206067].